Vector polarized ^{6}Li scattering from ^{12}C and ^{16}O

S. P. Van Verst,* D. P. Sanderson,† D. E. Trcka, K. W. Kemper, V. Hnizdo,‡ B. G. Schmidt, and K. R. Chapman
Department of Physics, Florida State University, Tallahassee, Florida 32306
(Received 20 September 1988)

The elastic scattering vector analyzing powers for ^{6}Li+^{16}O at 25.7 MeV and ^{6}Li+^{12}C at 30 MeV have been measured. In addition, measurement of the vector analyzing power for inelastic ^{6}Li scattering has been made for the 2^+ (4.44 MeV) state in ^{12}C. Excitation function data for ^{6}Li+^{16}O elastic and inelastic scattering have also been measured at five angles for ^{6}Li lab energies through the range 15–28 MeV in 375 keV steps. These data show the system to be resonance free at 25.7 MeV. The data have been analyzed in the coupled channels framework, employing the double folding model for the real part of the nuclear scattering potential. The coupling strengths in the coupled channels calculations were determined from inelastic scattering cross-section data directly. The elastic scattering vector analyzing powers arise from a complicated interference between channel coupling and spin-orbit contributions, whereas the ^{12}C, 2^+ inelastic vector analyzing power arises from the spin-orbit potential only. Inelastic scattering analyzing powers may allow the shape and strength of heavy-ion spin-orbit potentials to be investigated more clearly than do the elastic scattering analyzing powers. The normalization of the double-folded real potential was found to be in the range 0.85–1.00 in the coupled channel calculations, thus bringing the normalization of ^{6}Li scattering into agreement with other projectiles.

I. INTRODUCTION

Initially, it was expected that the vector analyzing power (VAP) for heavy-ion scattering would be small because it is only the outer, unpaired nucleons which contribute to the total nucleus-nucleus spin-orbit part of the interaction, and thus the strength of the spin-orbit potential should be reduced by $1/A$ relative to the central potential. However, measurements made with the Hamburg-Heidelberg polarized alkali ion source[1] had a surprisingly large VAP (Ref. 2) for ^{6}Li elastically scattered from several targets. The origin of the large VAP has been the subject of intense theoretical investigation over the past several years.

The first experiments with the polarized Li beam[2] measured the VAP for elastic ^{6}Li scattering from ^{12}C, ^{16}O, ^{28}Si, and ^{58}Ni at laboratory energies around 20 MeV. The analysis of these data concentrated on the determination of the ^{6}Li spin-orbit (SO) potential. Two early analyses of these data[2,3] considered ^{6}Li to be an $\alpha+d$ system and calculated cluster-folding model spin-orbit potentials using deuteron-target SO potentials from the literature. The order of magnitude of the data was understood within this framework, although it failed to describe the experimental data in detail. An analysis in which a double-folded ^{6}Li-target SO potential was calculated from an effective nucleon-nucleon interaction gave similar results to those mentioned above.[4]

An interesting twist to the ^{6}Li spin-orbit problem came when it was found[5] that the VAP for ^{7}Li+^{58}Ni had approximately the same size but opposite sign as the ^{6}Li+^{58}Ni data. This was in contradiction to the folding model prediction that the VAP for ^{7}Li would have the same sign but be smaller in magnitude than ^{6}Li. Altogether, these analyses left a confusing picture of the ^{6}Li spin-orbit interaction.

Nishioka *et al.*,[6] and independently Ohnishi *et al.*[7] and Petrovich *et al.*[8], came up with a novel picture which gives rise to a large vector analyzing power with no explicit spin-orbit potential present in the nucleus-nucleus interaction. They found that coupled channel (CC) effects arising from projectile excitation and reorientation made dominant contributions to the VAP and, in fact, explained the opposite signs of the measured VAP for ^{6,7}Li+^{58}Ni. Windham *et al.*[9] confirmed that the projectile excitation effect is an essential ingredient of polarized Li scattering in general in their analysis of ^{6}Li+^{16}O and ^{28}Si. For all three targets, significantly improved fits to the VAP data were obtained over single-channel calculations.

More recently, Sakuragi and co-workers[10,11] have shown that CC calculations employing double-folded potentials, as opposed to cluster-folded potentials, give improved fits to the ^{6}Li+^{16}O VAP data with no renormalization of the potential as found in single-channel calculations. In this analysis, the ^{6}Li ground state and first three $L=2$ inelastic transitions were included in the coupling, and the spin-orbit potential was not included. Sakuragi[11] concluded that by including more explicit channels in the coupling scheme, the need to include a spin-orbit term in the potential was removed. This result suggests that the heavy-ion spin-orbit potential may indeed be small, as initially predicted.

Although the channel-coupling effects seem to be essential in describing the VAP data, the fits to the elastic scattering cross section in the above analyses are poor.

For example, the predicted $^6Li+^{16}O$ cross section at 22.8 MeV is completely out of phase with the data. Another drawback of the CC analyses was the fact that the coupling strengths in the calculations were treated as free parameters since there was no inelastic cross-section data at the time with which to set the coupling strengths.

In the present work, VAP data are reported for $^6Li+^{16}O$ at 25.7 MeV, an energy which is close to previously reported data,[2] to ascertain if $^6Li+^{16}O$ scattering exhibits the same rapid fluctuations in both cross section and VAP observed for $^6Li+^{12}C$ near 20 MeV. The $^6Li+^{16}O$ system is the subject of many of the latest extensive theoretical calculations[10,11] that are being done to determine the origin of the large elastic VAP for ^6Li scattering. The specific energy of 25.7 MeV was selected because the ^6Li, 3^+ inelastic cross section has been measured previously at this energy,[12] and these data can be used to unambiguously determine the coupling strength in the calculations. In addition, excitation functions for $^6Li+^{16}O$ at five different angles have been measured.

The elastic scattering cross section for $^6Li+^{16}O$ at 22.8 MeV measured earlier at Heidelberg[2] has been extended out to 100° c.m. to provide more constraints on the calculations. Also at 22.8 MeV, the inelastic cross section for excitation of the ^6Li, 3^+ state has been measured and is reported here. For the $^6Li+^{16}O$ system, a data set now exists at two closely spaced energies which includes cross sections for elastic scattering, inelastic scattering to the 3^+ (2.18 MeV) state in ^6Li, and the elastic scattering VAP.

The elastic scattering VAP for $^6Li+^{12}C$ at 30 MeV and the VAP for inelastic scattering to the 2^+ (4.44 MeV) state in ^{12}C are also presented in this work. Again, this energy was chosen because the cross sections to the 3^+ (2.18 MeV) and 2^+ (4.31 MeV) states in ^6Li and the 2^+ (4.44 MeV) state in ^{12}C have been previously measured[12] and thus allow the determination of the coupling strengths for these states. Excitation functions measured by Fulton and Cormier[13] indicate the system to be resonance free at this energy. The results of a coupled-channels analysis of both sets of data employing the double-folding model for the real part of the central and spin-orbit scattering potentials are presented.

II. EXPERIMENTAL PROCEDURE

The measurements for the present work were carried out at the Florida State University (FSU) tandem Van de Graaff accelerator laboratory. A beam of vector polarized ^6Li ions, produced with the FSU polarized ion source, was accelerated and transported to a scattering chamber specifically designed to measure polarization observables and then into a polarimeter where the polarization of the beam was monitored throughout the experiment. The polarized source, based on the Heidelberg design,[1,2,14,15] employs the atomic beam method of selectively populating and separating certain hyperfine magnetic substates of the atom. Typically, 12 nA of $^6Li^{3+}$ is obtained on target, and the beam polarization was determined to be $\tau_{10}=-0.61\pm0.06$ in the transverse frame of reference. The Madison convention[16] is used throughout this work for the description of polarization observables.

The scattering chamber used a three-part collimation system which defined a 2-mm-diam beam spot on target. Two detector wedges, located on opposite sides of the beam, were mounted on rotating tables. Each wedge consisted of three silicon surface barrier detector systems separated by 7.5° so that data could be obtained simultaneously at three different scattering angles. The detectors were collimated such that they subtended a polar angle of 0.3° in the laboratory frame of reference.

At the exit of the scattering chamber, the beam passed through a thin Havar foil and entered the polarimeter,[17] which is a scattering chamber designed to monitor the beam polarization during experiments. The polarimeter was filled with He gas, thereby making use of the reaction $^6Li+^4He$. Two 500-μm surface barrier detectors, viewing a common region of gas, were placed symmetrically at a lab angle of 15° with respect to the beam. The polarimeter asymmetry was calculated at least every 5 min to make certain the beam polarization remained constant. The variation in the beam polarization was found to be less than 5%.

A primary concern in choosing a polarization monitor is finding a reaction which gives rise to a large left-right asymmetry, ϵ. Egelhof *et al.*[18] found that the asymmetry for $^6Li+^4He$ at 150° c.m. while high, decreases as the beam energy increases from 15 to 23 MeV. In the present work, it was found that ϵ was reduced by about a factor of 2 in going from a 20- to a 25.7-MeV ^6Li beam. In order to increase the sensitivity of the polarimeter at 25.7 MeV, an aluminum foil of thickness 0.0038 cm was placed just before the polarimeter entrance. Due to energy loss in the foil, the beam energy was reduced to 20.4 MeV. The resulting asymmetry for a 25.7-MeV beam passing through the Al foil was found to be identical to that for a 20-MeV beam with no foil. This indicates that the foil does not cause a loss of beam polarization, and is therefore a good method for increasing the sensitivity of the polarization monitor for higher energy beams. For the 30-MeV ^6Li beam, a second layer of Al foil was added to the original foil, again reducing the beam energy to about 20 MeV at the polarimeter entrance.

The VAP data were measured in the angular range from approximately 25° to 70° c.m. For the forward angle ($\theta_{lab}<35°$) ^{16}O measurements, a 200-$\mu g/cm^2$ SiO_2 target was used. The ^{16}O and ^{28}Si ground state peaks were well separated for scattering angles greater than $17°_{lab}$. At angles less than 17° the two ground-state peaks overlapped and the ^{16}O yield could not be accurately extracted. With the SiO_2 target, a problem arises around $\theta_{lab}=40°$ where the energy of the scattered ^6Li particles from the ^{28}Si (2^+), 1.78 MeV state overlaps the ^{16}O ground-state scattered particles. Therefore, 200-$\mu g/cm^2$ BeO targets were used for angles greater than 35° and extending out to $\theta_{lab}=49°$, where the small cross sections made it impractical to make further measurements. For the ^{12}C study, a 200-$\mu g/cm^2$ ^{12}C target was used for the entire range of data, extending from lab angles of 14° to 43°. Again, cross sections on the order of 0.1 mb/sr prevented taking data out to larger angles in reasonable counting times.

During the course of the present measurements, strong field transitions were not operational in the ion source so that it was not practical to flip the spin of the beam. Consequently, the quantity measured in the experiment is the left-right asymmetry $\epsilon[=(L-R)/(L+R)]$, which is proportional to the change in cross section due to the beam being polarized. Since the asymmetry, ϵ, depends on the difference between the yields in the left and right detectors and the elastic cross sections were varying rapidly, it was important that the detectors be placed at the same angle. To set the left and right detectors as close to the same angle as possible, the relative cross section for ^{6}Li+^{12}C at 30 MeV was measured from 30° to 40° in the center of mass with a detector on each side of the beam. This reaction[12] was chosen due to its highly oscillatory structure. At each angle where ϵ was determined with the polarized beam, the left and right yields were also measured with an unpolarized beam. Errors in ϵ were typically 0.05 and included statistical errors arising from both the polarized and unpolarized beam measurements.

The vector analyzing power for a reaction with a spin-1 projectile, such as ^{6}Li, is defined as

$$iT_{11}=\frac{\epsilon}{\sqrt{2}\tau_{10}},$$

where iT_{11} is in spherical tensor notation, τ_{10} is the beam polarization, and ϵ is the asymmetry for the reaction. It is ϵ that is measured experimentally, and then iT_{11} is calculated from the beam polarization and asymmetry.

The excitation function data for ^{6}Li+^{16}O were taken at center-of-mass angles of 47.3°, 56.7°, 130°, 146°, and 160°. The back-angle measurements were made by scattering an ^{16}O beam from a ^{6}Li target and detecting the recoil lithium nuclei. The ^{16}O energies corresponded to ^{6}Li laboratory beam energies between 15 and 28 MeV in 375-keV steps. Target condition, charge integration, and accelerator performance were monitored by detecting the elastic ^{16}O yields from a thin layer of gold backing on the targets.

The measured excitation function cross sections are shown in Fig. 1 for the three peaks containing the elastic, the unresolved 0^+ (6.05 MeV) and 3^- (6.13 MeV), and the unresolved 2^+ (6.92 MeV) and 1^- (7.12 MeV) states in ^{16}O. The data does indicate the occurrence of an anomalous structure at $\approx$21.25 MeV with a width of $\approx$2 MeV. This structure is present in the elastic channel at all three angles, in the $0^+,3^-$ channel at 160°, and the $2^+,1^-$ channel at 130°.

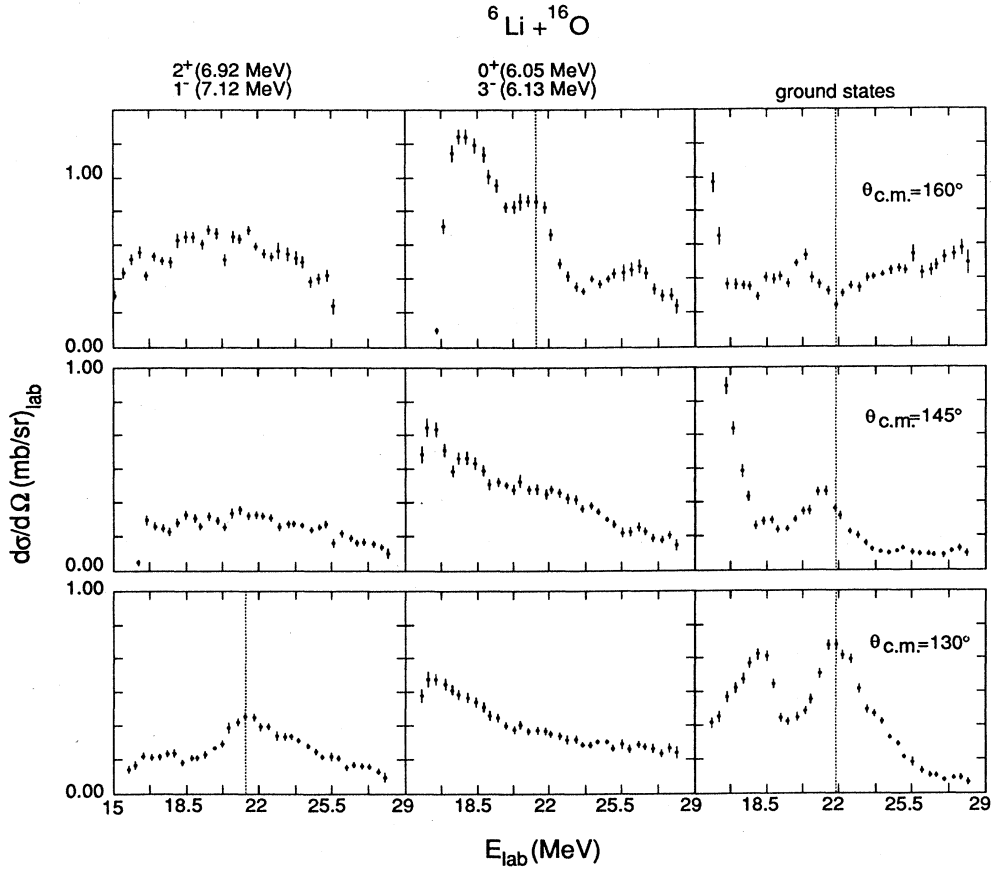

FIG. 1. Excitation functions for ^{6}Li+^{16}O elastic and inelastic scattering.

III. ANALYSIS

The purpose of the present analysis is to isolate the contribution from channel coupling to the elastic VAP, with emphasis on the excitation of ^{6}Li, by employing microscopic double-folded potentials. The standard references on these subjects are Tamura[19] for coupled channels, and Refs. 8 and 20 for the double-folding model.

The strength of the coupling to a particular channel is an input into the calculation. This coupling strength is often treated as a free parameter and is adjusted to give the best fit to elastic scattering data. Since the magnitude of the coupling strength is directly related to the influence that the inelastic channel has on the elastic scattering, an incorrect coupling strength will lead to meaningless results. In the present work, the coupling strengths were determined from experimental data whenever possible.

A. ^{6}Li+^{16}O: optical model analysis

Optical model calculations for ^{6}Li+^{16}O were carried out for data taken at the two closely spaced energies of 22.8 and 25.7 MeV to determine if a single-channel calculation with a spin-orbit interaction could describe the elastic cross section and VAP data at both energies with little or no change in potential parameters. The presence of rapidly varying parameters to describe the data could be a sign that processes other than direct scattering contribute to the elastic scattering. The data were analyzed in terms of the optical model using double-folded (DF) real central and phenomenological imaginary central potentials and phenomenological real and imaginary spin-orbit potentials. The double-folding model[20] provided a fundamental approach which related the nucleus-nucleus potential to the underlying nucleon-nucleon interaction and the properties of the colliding nuclei. Since there is no theoretical model which allows the imaginary contribution to the potential to be calculated in an unambiguous fashion, a standard Woods-Saxon shape was used, with the depth, radius, and diffuseness being free parameters.

The real central DF potential was obtained by folding the projectile and target matter densities with an effective nucleon-nucleon interaction. In this work, the M3Y interaction of Bertsch *et al.*,[21] modified to account for single nucleon knockout exchange,[22] was chosen. The ^{6}Li matter density was obtained from the measured charge density of Suelzle *et al.*[23] by unfolding the finite charge distribution of the proton and assuming the proton and neutron densities to be identical. A harmonic oscillator density was assumed for ^{16}O. Details of the calculation of the DF potential are given in Ref. 12.

For the real and imaginary spin-orbit potential, a Thomas form was used, given by

$$V^{LS}(r)=\left[\frac{\hbar}{m_\pi c}\right]^2 \frac{V_0}{r}\frac{d}{dr}\left\{\left[1+\exp\left[\frac{r-r_{LS}A_t^{1/3}}{a_{LS}}\right]\right]^{-1}\right\}\mathbf{l}\cdot\mathbf{s}\ .$$

The optical model computer code HERMES (Ref. 24) was used to calculate the elastic scattering cross section and VAP. All potential parameters were allowed to vary, including the normalization of the DF potential, to obtain the best fit to the data. The parameters of Ref. 12 were used as a starting point.

Calculations using the parameters found to give the best fit at 25.7 MeV are shown at both 25.7 and 22.8 MeV as the solid lines in Fig. 2 for the elastic cross section and Fig. 3 for the elastic VAP. The potential parameters are

TABLE I. Potential parameters. The definition of the potentials is given in Ref. 24. The interaction radii are given by $R_x = r_x A_t^{1/3}$.

	^{6}Li+^{16}O				^{6}Li+^{12}C		
Parameter	DF-WS	WS-WS	CC	CC SO	DF-WS	CC	CC SO
N	0.65		1.0	1.0	0.73	0.85	0.85
V (MeV)		124.8					
r_R (fm)		1.15					
a_R (fm)		0.91					
W (MeV)			7.1	5.1	8.78	8.0	8.0
W_D (MeV)	9.69	7.33					
r_I (fm)	1.74	1.79	2.3	2.3	2.13	2.03	2.03
a_I (fm)	0.75	0.82	0.80	0.70	0.76	0.78	0.78
V_{LS} (MeV)	1.62	1.07		3.4	1.33		5.1
r_{RLS} (fm)	1.36	1.46		1.22	1.11		1.20
a_{RLS} (fm)	0.45	0.49		0.71	0.37		0.65
W_{LS} (MeV)	−1.0	−1.0					
r_{ILS} (fm)	1.32	1.32					
a_{ILS} (fm)	0.50	0.50					

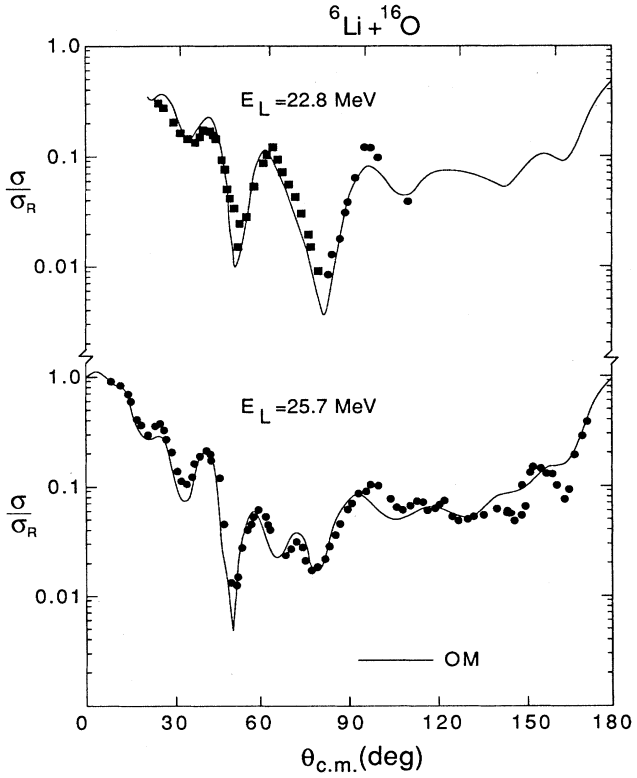

FIG. 2. Optical model calculations for ^{6}Li+^{16}O elastic scattering at 22.8 (top) and 25.7 MeV (bottom). The same set of potential parameters was used at both energies. The circle data points are from the present work. The square data points are from Ref. 2.

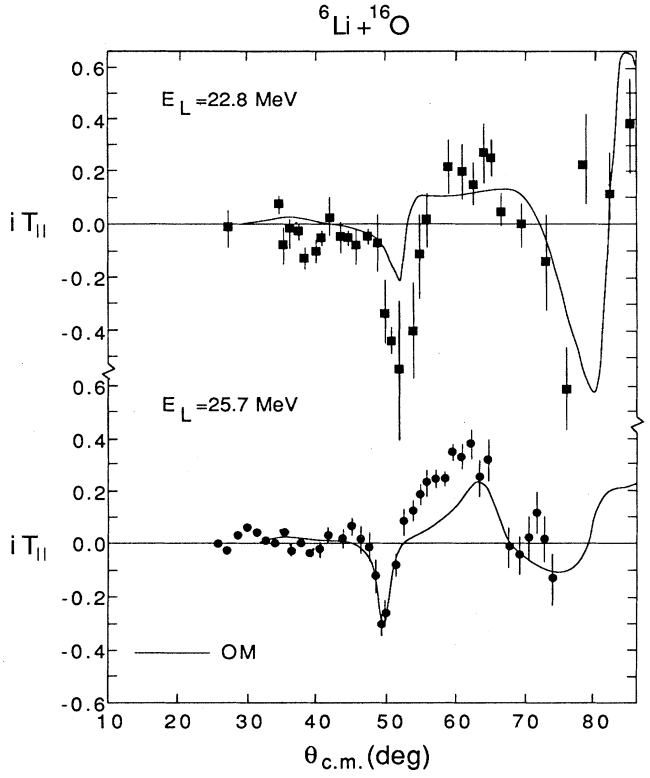

FIG. 3. Optical model calculations for the ^{6}Li+^{16}O elastic vector analyzing power at 22.8 (top) and 25.7 MeV (bottom). These results come from the same calculations as in Fig. 2. The 22.8-MeV data are from Ref. 2, while the 25.7-MeV data are from the present work.

given in Table I as set DF-WS (where WS indicates the Woods-Saxon form). The calculation gives a reasonable fit to all four sets of data, indicating that the scattering arises from direct reaction processes. The excitation function for ^{6}Li+^{16}O, shown at two forward angles in Fig. 4 is another indication that the scattering arises from direct reaction processes. The energy region around 26 MeV seems to be clear of the resonance structures observed in the excitation function data.

A weak imaginary spin-orbit potential, opposite in sign to the imaginary central potential, was found to give an improved fit to the VAP data. Similar results have been observed in polarized deuteron scattering.[25]

Optical model calculations were also carried out using a volume Woods-Saxon (WS) form for the real central potential and either a volume or surface WS form for the imaginary central potential. It is convenient to have the optical potential parametrized in terms of WS shapes so that other researchers can easily use the potential for other studies, such as distorted-wave Born approximation (DWBA) calculations. These calculations gave descriptions of the data similar to those discussed above, with the surface WS imaginary potential giving a slightly better fit to both the elastic cross section and VAP. These potential parameters are listed in Table I as set WS-WS. The calculated angular distributions are not shown because they are indistinguishable from those shown in Figs. 2 and 3.

B. ^{6}Li+^{12}C: optical model analysis

The optical model calculations, using a double-folded real potential, for ^{6}Li+^{12}C at 30 MeV were carried out

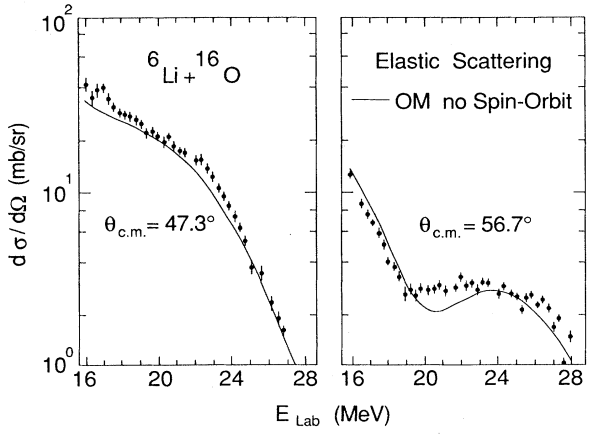

FIG. 4. ^{6}Li+^{16}O elastic excitation function data with the optical model calculation described in the text.

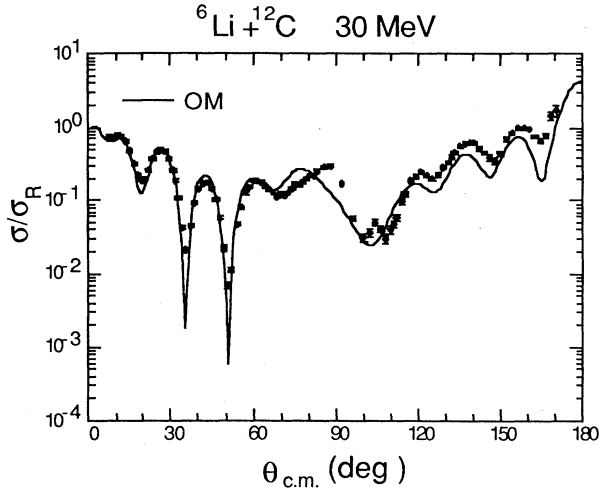

FIG. 5. Optical model calculation for ^{6}Li+^{12}C elastic scattering at 30.0 MeV over full angular range for which data have been measured.

following the procedure described in the preceding section. The resulting best fits are shown in Fig. 5 for the elastic scattering cross section over the whole angular range for which data are available, and Fig. 6 for the elastic scattering and VAP over the same angular range. The potential parameters are given in Table I as set DF-WS. An imaginary spin-orbit potential did not improve the description of the data.

The optical model was unable to give a good description of the elastic VAP data. The first negative structure was predicted quite well; however, the calculation predicted a second structure that was not seen in the data.

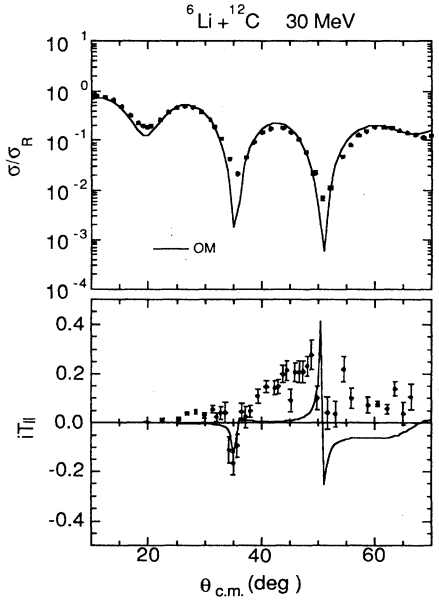

FIG. 6. Angular distribution of the elastic scattering cross section and elastic vector analyzing power for ^{6}Li+^{12}C at 30.0 MeV. The curve is the optical model calculation.

Because of this calculation, the data were taken several times in the region of the predicted second dip to search for its presence. As can be seen from Fig. 6, the excursions in the predicted VAP correspond to the minima in the elastic cross section data. The fact that the second structure was not observed in the elastic VAP data is an indication that more complicated processes, such as channel coupling, were important in the scattering.

C. ^{6}Li+^{16}O: coupled channels analysis

The coupled channels code CHUCK (Ref. 26) was used to calculate the elastic and inelastic cross sections and the elastic VAP to investigate the effects of channel coupling on the elastic VAP. Couplings to both the 3^+ (2.18 MeV) and 2^+ (4.31 MeV) states in ^{6}Li were included in the calculation. Since the 2^+ cross-section data has not been measured for ^{6}Li+^{16}O, the coupling strength was assumed to be the same as determined for ^{6}Li+^{12}C at 30 MeV. Initially, the calculations contained no explicit spin-orbit term.

The real part of the nuclear transition potential was obtained by folding the M3Y interaction with the quadrupole transition density for excitation of the 3^+ state in ^{6}Li and the ground-state matter density of ^{16}O. The $l=2$ transition density was assumed to have the derivative form

$$\rho_2(r) = -\delta_2^{ij}\frac{d}{dr}\rho_0(r) ,$$

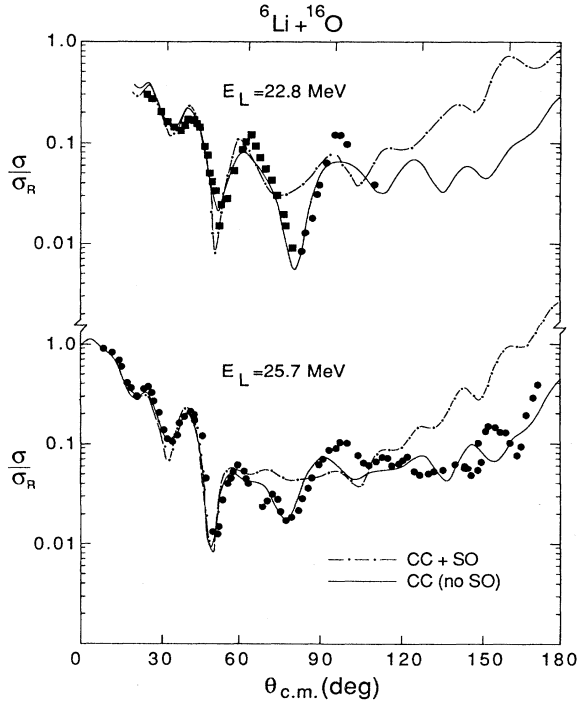

FIG. 7. Results of CC calculations, including coupling to the ^{6}Li, 3^+ state only, of the elastic scattering cross section for ^{6}Li+^{16}O. The solid curve has no spin-orbit potential and the dot-dashed curve employs the double-folded spin-orbit potential of Ref. 4.

where $\rho_0(r)$ is the ^{6}Li ground-state matter density and δ_2^{ij} is the quadrupole deformation length for the transition from state i to state j. The value of the deformation length for the transition to the 3^+ state in ^{6}Li, δ_2^{01}, was adjusted until the magnitude of the calculated inelastic cross section reproduced the data.

The imaginary part of the transition potential was taken to be the derivative of the diagonal Woods-Saxon potential multiplied by a deformation length. The deformation lengths for the real and imaginary terms were made to be equal. Coulomb excitation was also included in the transition potential.

The first calculations carried out included only the ^{6}Li, 3^+ state in the coupling scheme. With the normalization of the DF potential set to $N=0.65$, no results were obtained that described the elastic scattering data, even at forward angles, when only the imaginary potential was varied. By optimizing the parameters N, W, r_I, and a_I in the CC calculation, it was found that $N=1$ gave the best description of the forward-angle elastic scattering cross section. The best fit was arrived at by setting up a grid on the parameters to be varied. Calculations were then carried out for all points on the grid, and the result which gave the best fit at forward angles was chosen.

The results of this calculation at 22.8 and 25.7 MeV, with no explicit spin-orbit term, are shown as the solid lines in Fig. 7 for the elastic cross section and in Fig. 8 for the elastic VAP. The parameters are listed as set CC in Table I. The elastic scattering is described quite well at angles less than 90° c.m. The channel coupling gives rise to a large analyzing power with no explicit spin-orbit interaction, although a defect exists in the model as is seen by the large spike in the predicted elastic VAP around 45° c.m. Data were measured several times in this angular range to make certain the spike did not exist experimentally. The predictions for the 3^+ cross sections are shown in Fig. 9. The coupling strength was set to reproduce the correct magnitude of the 3^+ data. The resulting deformation length is $\delta_2^{01}=2.34$ fm, compared to 3.69 fm determined from the $B(E2)$ value.

A calculation investigating the reorientation of the ^{6}Li, 3^+ state was also carried out. In an earlier analysis,[12] a reorientation deformation length δ_2^{11} equal to one-half that for the 1^+ to 3^+ transition was assumed. The calculations of the elastic scattering cross section in the region from 60° to 100° c.m. required a negative value of δ_2^{11} to describe the data. In the present work it was found that the elastic VAP was very sensitive to the reorientation and, like the elastic scattering cross section, also requires a negative value for the deformation length. The fit to the data in the angular region sensitive to the reorientation was not good enough to determine the magnitude of the reorientation strength. However, the descriptions of both the elastic scattering cross section and VAP were far worse with positive values of the deformation length. For values of δ_2^{11} less than one-fourth of δ_2^{01} the calculation was similar to one with no reorientation term, while values greater than one-fourth resulted in far worse descriptions of the data.

Coupled channel calculations were also carried out with a real spin-orbit interaction included. The double-folded spin-orbit potential of Petrovich *et al.*[4] given in the form of an equivalent Woods-Saxon potential, was

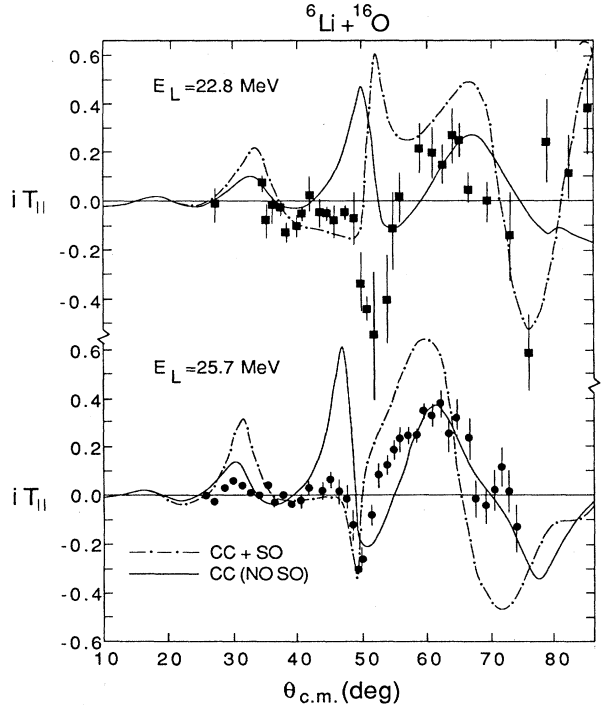

FIG. 8. Results of CC calculations of the elastic vector analyzing power for ^{6}Li + ^{16}O. The curves are as in Fig. 7.

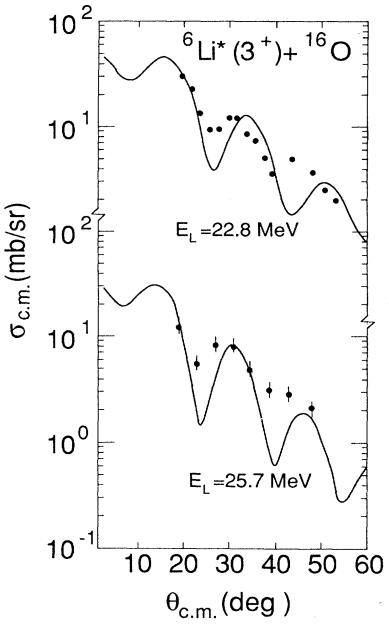

FIG. 9. Results of the CC calculation of Fig. 7 for the ^{6}Li (3^+) cross section. This state was not sensitive to the spin-orbit potential. The ^{6}Li (3^+) data are from Ref. 12.

used in the calculation and was considered fixed and not varied. The resulting calculation, with the parameters W, r_I, and a_I optimized is shown as the dot-dashed line in Figs. 7 and 8 and the parameters are given as set CC SO in Table I. Although the forward-angle elastic scattering cross section was reproduced quite well, the backward angles were overpredicted by an order of magnitude. This can be attributed to the decrease in the imaginary potential required to improve the fit to the elastic cross section in the angular region from 60° to 100° c.m. No attempt was made to improve the large angle fit since it has been shown[11,27] that this angular region is sensitive to direct breakup effects, which are not treated explicitly here.

These calculations show that the elastic VAP arises from an interference between the effects of channel coupling and the spin-orbit interaction. The addition of the spin-orbit potential had the important effect of damping out the spike in the analyzing power at 50°c.m. which was present in the CC results with no spin-orbit potential. The 3^+ cross section was not sensitive to the addition of the spin-orbit potential.

Calculations were also carried out including the 2^+ (4.31 MeV) state in ^{6}Li. Since the inelastic cross section for that state had not been measured, the coupling strength was set to that determined from the ^{6}Li+^{12}C analysis in Sec. III D. The 2^+ state was found to be very important in describing the VAP (dotted curve in Fig. 10). Including both the 2^+ and 3^+ states gave a much better prediction of the data than when only the 3^+ state was included. Importantly, this calculation gave an improved fit to the dip in the elastic VAP around 50°, and it also predicted the correct magnitude of the back-angle rise in the data.

D. ^{6}Li+^{12}C: coupled channels analysis

The coupled channels analysis of the ^{6}Li+^{12}C study followed the procedure described above for ^{6}Li+^{16}O. For the ^{12}C case, inelastic cross sections to both the 3^+ (2.18 MeV) and 2^+ (4.31 MeV) states in ^{6}Li have been previously measured.[12] Therefore, coupling to both these states was investigated. Additionally, the strongly excited 2^+ (4.44 MeV) state in ^{12}C was also taken into account.

Initial calculations, including coupling to the 3^+ and 2^+ states in ^{6}Li, showed that $N=0.85$ for the normalization of the DF potential gave the best description of the forward-angle elastic data. Results of calculations employing various coupling schemes are shown in Fig. 11 for the elastic scattering cross section and Fig. 12 for the elastic VAP, and in Fig. 13 for the inelastic ^{6}Li scattering. The potential parameters are given in Table I as set CC. A spin-orbit term was not included in these calculations. The coupling strength for each state was determined by fitting the calculation to the magnitude of the inelastic cross section. The resulting deformation lengths were 1.89 fm for coupling to the 3^+ state in ^{6}Li, 0.95 fm for reorientation of the 3^+ state in ^{6}Li, 2.13 fm for the 2^+ state in ^{6}Li, and 1.58 fm for coupling to the 2^+ state in ^{12}C. For comparison (see Table II), the corresponding deformation lengths derived from the $B(E2)$ values were 3.69, 1.85, 1.83, and 1.48 fm, where the reorientation deformation length was assumed to be one-half that for coupling the ground state to the 3^+ state. In addition, Table II also shows the deformation lengths for the states in ^{6}Li obtained from proton scattering results.

For the elastic scattering cross section, including the coupling to the ^{6}Li (2^+) state gave a much better description of the data than when only the ^{6}Li (3^+) state was included. The first three forward-angle oscillations and the back-angle data were described quite well (dashed line). As can be seen, including the ^{12}C (2^+) state did not change the calculation. All three results failed to de-

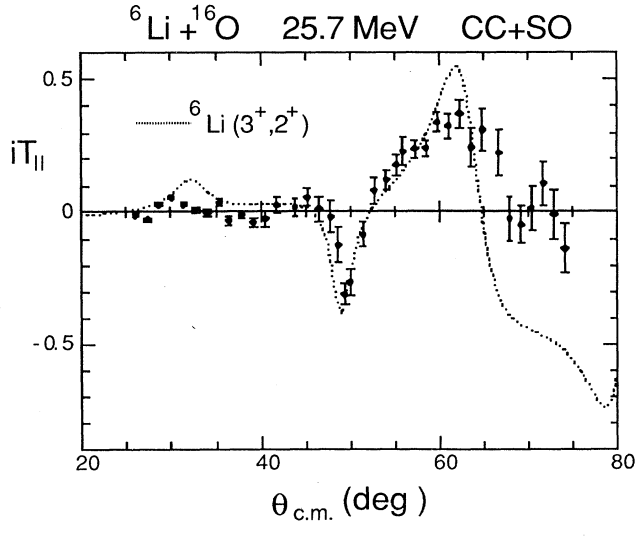

FIG. 10. Results of a CC calculation for ^{6}Li+^{16}O elastic vector analyzing power at 25.7 MeV. The curve includes the spin-orbit potential and coupling to the 3^+ and 2^+ states in ^{6}Li.

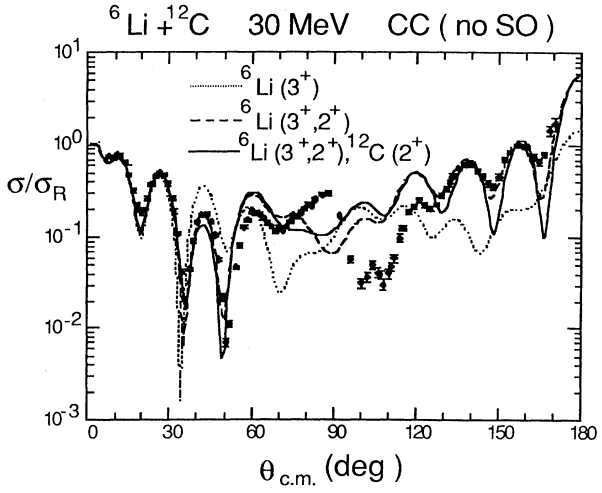

FIG. 11. Results of CC calculations employing various coupling schemes for ^{6}Li+^{12}C at 30 MeV. The calculation does not include an explicit spin-orbit interaction.

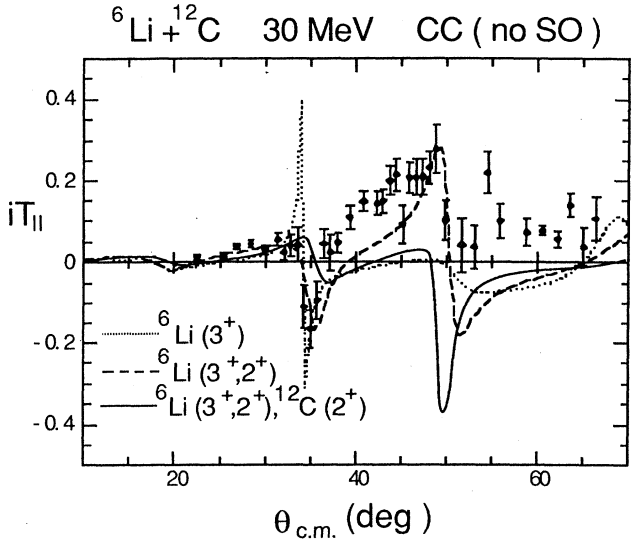

FIG. 12. Results of CC calculations employing the coupling schemes of Fig. 11 for the ^{6}Li+^{12}C elastic vector analyzing power at 30.0 MeV. The calculations do not contain an explicit spin-orbit potential.

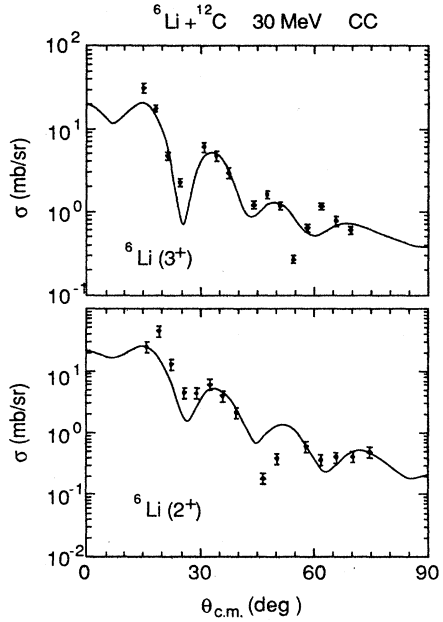

FIG. 13. The full CC calculation with no spin-orbit potential for the 3^+ (top) and 2^+ states in ^{6}Li. The experimental data are from Ref. 12.

scribe the midangle region around 90° c.m. It is clear that both the 3^+ and 2^+ states in ^{6}Li needed to be included in the coupling scheme. This is consistent with the results obtained in the ^{6}Li+^{16}O study.

The elastic VAP data also showed the need to include the ^{6}Li (2^+) state. The large spike around 35° c.m. that occurred when only the 3^+ state was considered was damped out by adding the 2^+ state. Also, the $3^+,2^+$ calculation (dashed curve) gave a reasonable description of the data from 40° to 50° c.m., whereas the 3^+ calculation (dotted curve) predicted zero analyzing power in that angular range. Unlike the elastic scattering cross section, the elastic VAP is quite sensitive to the ^{12}C (2^+) state. Including this state in the calculation destroys the fit for angles greater than 35° c.m. It is obvious from these results that some important physics was probably being missed in this analysis.

The cross-section data for the 3^+ and 2^+ states in ^{6}Li are shown in Fig. 13, and for the 2^+ state in ^{12}C in Fig. 14. The curves are the full CC calculations including all three channels with no spin-orbit term. It was found that any particular inelastic cross section was not sensitive to the effects of coupling in the other channels. The ^{6}Li states are described well, while only angles less than 60° c.m. are described for the 2^+ state in ^{12}C. No parameter combination was found which increased the magnitude of the back-angle prediction for the 4.4-MeV state.

Calculations were also carried out with the full coupling scheme and the double-folded spin-orbit potential for ^{6}Li+^{12}C of Ref. 4, and the results are shown in Figs. 15 and 16 for the elastic scattering cross section and elastic VAP. The parameters are listed in Table I. In both cases, the addition of the spin-orbit interaction resulted in a worse description of the data. This is in contrast to the ^{16}O target where the spin-orbit improved the fit to the data. The inelastic cross sections were not sensitive to the spin-orbit term in the optical potential.

Figure 17 shows the VAP for the 2^+ state in ^{12}C. The dotted curve is the result of the full CC calculation with no spin-orbit potential, which interestingly predicted zero analyzing power in the angular range of the data. Therefore, for the 2^+ state, the VAP was not due to an interference between the spin-orbit potential and coupling effects, but rather arose from the spin-orbit potential alone. The solid curve is the result of the full CC calculation including the Petrovich[4] double-folded spin-orbit po-

TABLE II. Deformation lengths (in fm).

System	^{6}Li($1^+\rightarrow3^+$)	^{6}Li($1^+\rightarrow2^+$)	^{16}O($0^+\rightarrow3^-$)	^{12}C($0^+\rightarrow2^+$)
^{6}Li+^{16}O	2.34	2.13	1.55	
^{6}Li+^{12}C	1.89	2.13		1.58
^{6}Li+p[a]	2.95	1.46		
$B(EL)$[b]	3.69	1.83	1.55	1.48

[a]Reference 28.
[b]Deformation lengths determined from the $B(EL)$ value; see Ref. 12 for details.

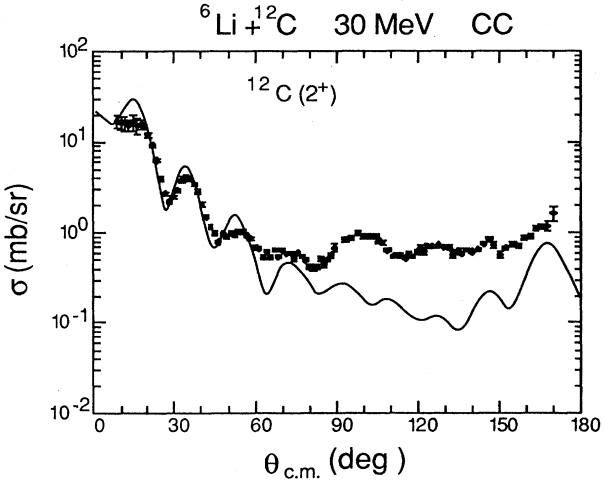

FIG. 14. The full CC calculation with no spin-orbit potential for the 2^+ state in ^{12}C. The experimental data are from Ref. 12.

tential. As can be seen from the figure, this calculation did a reasonable job describing the 2^+ analyzing power. These data may be important in the future for helping to pinpoint the magnitude of the heavy-ion spin-orbit potential.

IV. CONCLUSION

Vector analyzing powers have been measured for the elastic scattering of ^{6}Li+^{16}O at 25.7 MeV and ^{6}Li+^{12}C at 30 MeV and for the 4.44-MeV state in ^{12}C. The data were taken in small angular increments to map out the highly oscillatory structure of the analyzing powers. The present data, along with previous measurements, provided a severe test of current heavy-ion scattering models. It is especially worth noting that the ^{6}Li+^{16}O data now existed at two closely spaced energies so that the sensitivity of the analysis to resonances was checked. The previous

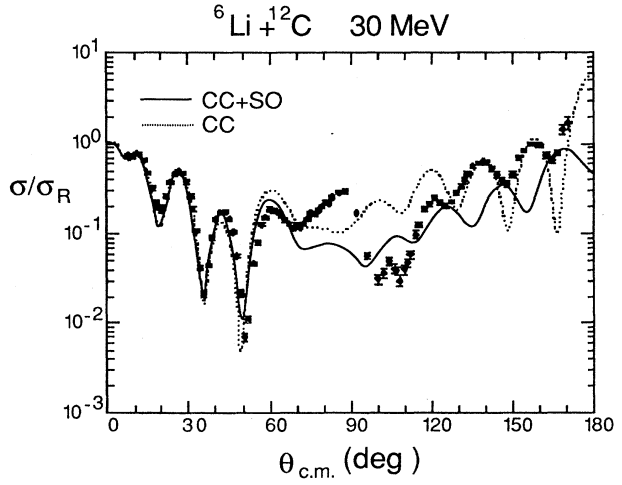

FIG. 15. Results of the full CC calculation with (solid curve) and without (dotted curve) an explicit spin-orbit potential for ^{6}Li+^{12}C elastic scattering.

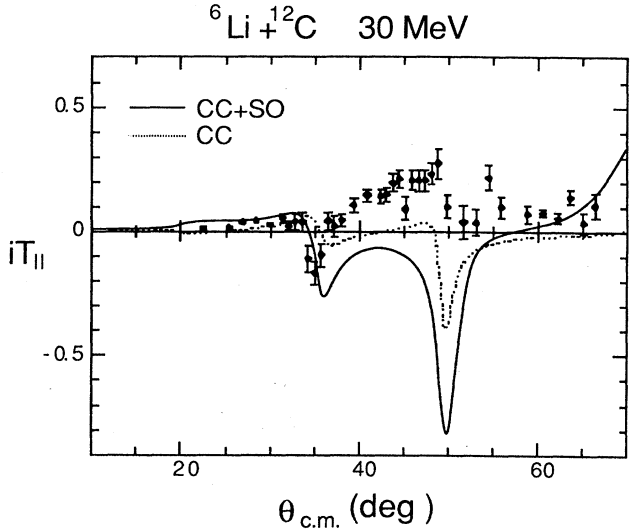

FIG. 16. The same as in Fig. 15 for the elastic vector analyzing power.

^{12}C data[2] have a rapidly changing VAP at 20 and 22.8 MeV that cannot be easily understood. In this same energy region, the excitation function data for large angle ^{6}Li+^{16}O scattering to the ^{16}O ground and excited states showed an anomalous fluctuation on the order of 100% located at a ^{6}Li beam energy of 21.25 MeV. The energy region around 25.7 MeV seemed to be clear from resonance contributions to the scattering.

The data were analyzed in the coupled channels framework, employing the double-folding model for the real part of the nuclear scattering potential. The folded potential was based on physical properties of the interacting nuclei determined from experiment. The coupling

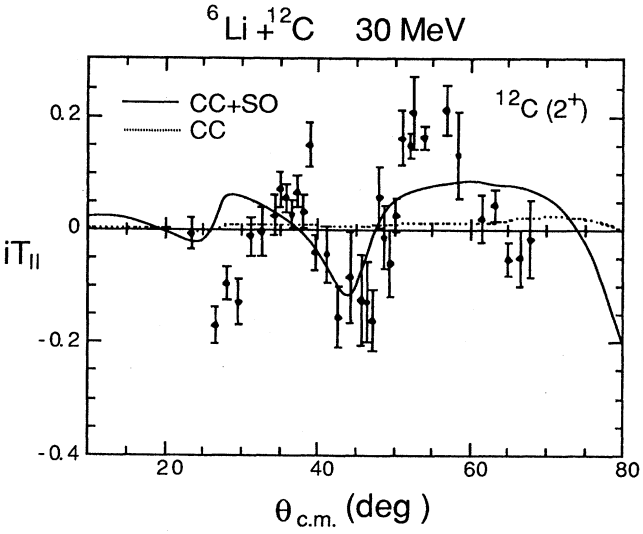

FIG. 17. The same as in Fig. 15 for the ^{12}C (2^+) vector analyzing power. Note that the calculation with no spin-orbit potential predicts a small analyzing power.

strengths in the CC calculations were unambiguously determined from inelastic scattering cross-section data. In addition, the double-folded spin-orbit potential[4] was used to eliminate any free parameters in the spin-dependent part of the interaction. The only free parameters in the calculations were the imaginary part of the potential and the strength of the folded central potential. The normalization of the double-folded potential was found to range from 0.85 to 1.0 in the present CC calculations. The channel coupling effects thus alleviate the renormalization anomaly found in optical model analyses of ^{6}Li elastic scattering.

It is quite clear from the present analysis that the vector analyzing power arises from a complicated interference between coupled channels effects and the spin-orbit interaction. For both the ^{16}O and ^{12}C targets, inclusion of both the 3^+ and 2^+ states in ^{6}Li gave improved fits to the data over calculations with the 3^+ state only.

The ^{6}Li+^{16}O elastic VAP data were described reasonably well within the coupled channels framework. The calculations clearly showed that an explicit spin-orbit potential was necessary to describe the data. The CC calculations were unable to correctly describe the ^{6}Li+^{12}C elastic VAP data.

Interestingly, the coupled channel calculations for the ^{12}C, 2^+ state predicted zero analyzing power in the angular range of the data, while the data varied in magnitude from 0.0 to ± 0.2. The inelastic VAP was reasonably well described when a spin-orbit potential was included in the calculations. These data may allow the shape and strength of the heavy-ion spin-orbit potential to be investigated more closely since there is no interference from coupling effects.

In comparing the previous Heidelberg ^{12}C data at 20 and 22.8 MeV with the current 30-MeV data, it is clear that the elastic VAP is decreasing in magnitude as the beam energy increases. At higher beam energies, many more channels will be open in the scattering process and thus the influence of any one particular channel will decrease. Indeed, CC calculations with no spin-orbit potential at 50 MeV show that the VAP arising from channel coupling is drastically reduced in magnitude at angles that are experimentally accessible. In the present work, it is difficult to isolate spin-orbit potential information due to its interference with coupling effects. Perhaps future efforts should be made to measure the VAP at higher energies where channel coupling effects may not be as important.

ACKNOWLEDGMENTS

The authors wish to thank T. B. Clegg, T. R. Ophel, P. A. Quin, and E. Steffens for many experimental suggestions. They would also like to thank J. A. Carr, F. Petrovich, R. J. Philpott, and D. Robson for providing a more complete understanding of the details of the analysis presented. One of the authors (V.H.) acknowledges the receipt of a sabbatical grant from the Foundation for Research Development, South Africa. The support of the National Science Foundation and the State of Florida is gratefully acknowledged.

*Present address: Nuclear Physics Laboratory, University of Washington, Seattle, WA 98195.

†Present address: National Superconducting Cyclotron Laboratory, Michigan State University, East Lansing, MI 48824.

‡Permanent address: Department of Physics and Schonland Research Centre for Nuclear Sciences, University of the Witwatersrand, Johannesburg, South Africa.

[1]E. Steffens, W. Dreves, H. Ebinghaus, M. Köhne, F. Fiedler, P. Egelhof, G. Engelhardt, D. Kassen, R. Schäfer, W. Weiss, and D. Fick, Nucl. Instrum. Methods **143**, 409 (1977).

[2]W. Weiss, P. Egelhof, K. D. Hildenbrand, D. Kassen, M. Makowska-Rzeszutko, D. Fick, H. Ebinghaus, E. Steffens, A. Amakawa, and K.-I. Kubo, Phys. Lett. **61B**, 237 (1976).

[3]H. Amakawa and K.-I. Kubo, Nucl. Phys. **A266**, 521 (1976).

[4]F. Petrovich, D. Stanley, L. A. Parks, and P. Nagel, Phys. Rev. C **17**, 1642 (1978).

[5]G. Tungate, R. Böttger, P. Egelhof, K.-H. Möbius, Z. Moroz, E. Steffens, W. Dreves, I. Koenig, and D. Fick, Phys. Lett. **98B**, 347 (1981).

[6]H. Nishioka, R. C. Johnson, J. A. Tostevin, and K.-I. Kubo, Phys. Rev. Lett. **48**, 1795 (1982); H. Nishioka, J. A. Tostevin, R. C. Johnson, and K.-I. Kubo, Nucl. Phys. **A415**, 230 (1984).

[7]H. Ohnishi, M. Tanifuji, M. Kamimura, Y. Sakuragi, and M. Yahiro, Nucl. Phys. **A415**, 271 (1984).

[8]F. Petrovich, R. J. Philpott, A. W. Carpenter, and J. A. Carr, Nucl. Phys. **A425**, 609 (1984).

[9]G. Windham, H. Nishioka, J. A. Tostevin, and R. C. Johnson, Phys. Lett. **138B**, 253 (1984).

[10]Y. Sakuragi, M. Kamimura, M. Yahiro, and M. Tanifuji, Phys. Lett. **153B**, 372 (1985).

[11]Y. Sakuragi, Phys. Rev. C **35**, 2161 (1987).

[12]M. F. Vineyard, J. Cook, and K. W. Kemper, Phys. Rev. C **31**, 879 (1985).

[13]B. R. Fulton and T. M. Cormier, Phys. Lett. **97B**, 209 (1980).

[14]H. Ebinghaus, U. Holm, H. V. Klapdor, and H. Neuert, Z. Phys. **199**, 68 (1967).

[15]R. Böttger, P. Egelhof, K.-H. Möbius, D. Presinger, E. Steffens, W. Dreves, B. Horn, I. Koenig, and D. Fick, Z. Phys. A **299**, 291 (1981).

[16]*Polarization Phenomena in Nuclear Reactions,* edited by H. H. Barschall and W. Haeberli (University of Wisconsin Press, Madison, 1971).

[17]R. R. Cadmus, Jr., The University of Wisconsin Report, Aug. 1975 (unpublished); R. R. Cadmus, Jr. and W. Haeberli, Nucl. Instrum. Methods **129**, 403 (1975).

[18]P. Egelhof, J. Barrette, P. Braun-Munzinger, W. Dreves, C. K. Gelbke, D. Kassen, E. Steffens, W. Weiss, and D. Fick, Phys. Lett. **84B**, 176 (1979).

[19]T. Tamura, Rev. Mod. Phys. **37**, 679 (1965).

[20]G. R. Satchler and W. G. Love, Phys. Rep. **55**, 183 (1979).

[21]G. Bertsch, J. Borysowicz, H. McManus, and W. G. Love, Nucl. Phys. **A284**, 399 (1977).

[22]M. Golin, F. Petrovich, and D. Robson, Phys. Lett. **64B**, 253 (1976).

[23]L. R. Suelzle, M. R. Yearian, and H. Crannell, Phys. Rev. **162**, 992 (1967).

[24]J. Cook, Comp. Phys. Commun. **31**, 363 (1984).

[25]R. P. Goddard and W. Haeberli, Phys. Rev. Lett. **40**, 701

(1978).
[26]P. D. Kunz, University of Colorado Report (unpublished), with modifications to program by J. R. Comfort, J. Cook, and V. Hnizdo.
[27]I. J. Thompson and M. A. Nagarajan, Phys. Lett. **106B**, 163 (1981).
[28]F. Petrovich, R. H. Howell, C. H. Poppe, S. M. Austin, and G. M. Crawly, Nucl. Phys. **A383**, 355 (1982).